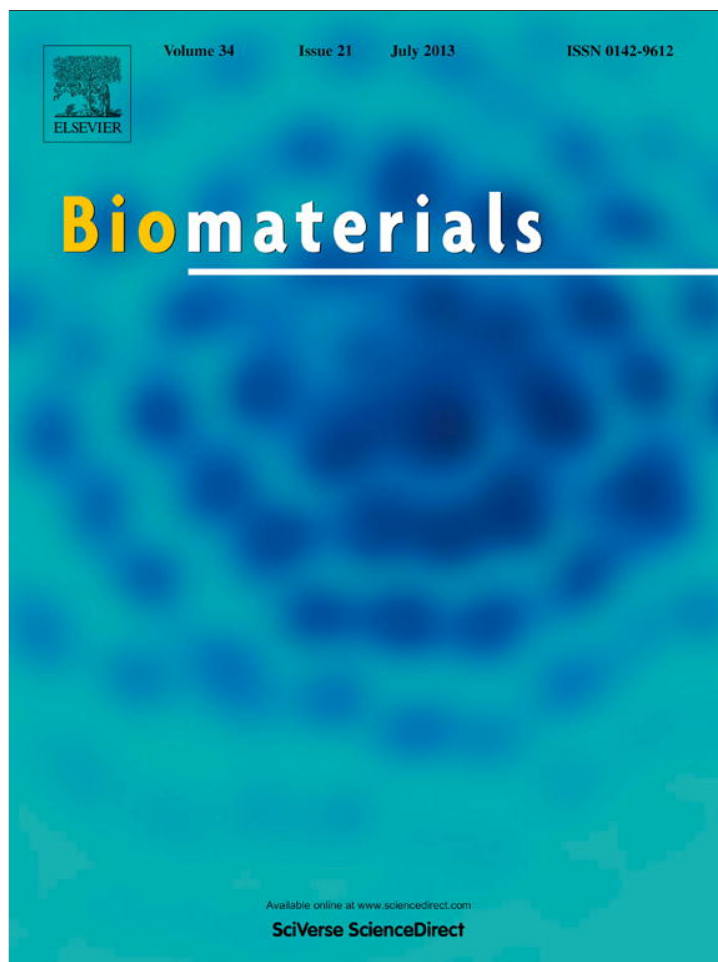


Provided for non-commercial research and education use.
Not for reproduction, distribution or commercial use.



This article appeared in a journal published by Elsevier. The attached copy is furnished to the author for internal non-commercial research and education use, including for instruction at the authors institution and sharing with colleagues.

Other uses, including reproduction and distribution, or selling or licensing copies, or posting to personal, institutional or third party websites are prohibited.

In most cases authors are permitted to post their version of the article (e.g. in Word or Tex form) to their personal website or institutional repository. Authors requiring further information regarding Elsevier's archiving and manuscript policies are encouraged to visit:

<http://www.elsevier.com/authorsrights>



Contents lists available at SciVerse ScienceDirect

Biomaterials

journal homepage: www.elsevier.com/locate/biomaterials

Inhalable magnetic nanoparticles for targeted hyperthermia in lung cancer therapy

Tanmoy Sadhukha^a, Timothy S. Wiedmann^a, Jayanth Panyam^{a,b,*}^a Department of Pharmaceutics, College of Pharmacy, University of Minnesota, Minneapolis, MN 55455, United States^b Masonic Cancer Center, University of Minnesota, Minneapolis, MN 55455, United States

ARTICLE INFO

Article history:

Received 4 February 2013

Accepted 20 March 2013

Available online 13 April 2013

Keywords:

Superparamagnetic iron oxide

Magnetic hyperthermia

EGFR

Inhalation delivery

Lung cancer

ABSTRACT

Lung cancer (specifically, non-small cell lung cancer; NSCLC) is the leading cause of cancer-related deaths in the United States. Poor response rates and survival with current treatments clearly indicate the urgent need for developing an effective means to treat NSCLC. Magnetic hyperthermia is a non-invasive approach for tumor ablation, and is based on heat generation by magnetic materials, such as superparamagnetic iron oxide (SPIO) nanoparticles, when subjected to an alternating magnetic field. However, inadequate delivery of magnetic nanoparticles to tumor cells can result in sub-lethal temperature change and induce resistance while non-targeted delivery of these particles to the healthy tissues can result in toxicity. In our studies, we evaluated the effectiveness of tumor-targeted SPIO nanoparticles for magnetic hyperthermia of lung cancer. EGFR-targeted, inhalable SPIO nanoparticles were synthesized and characterized for targeting lung tumor cells as well as for magnetic hyperthermia-mediated antitumor efficacy in a mouse orthotopic model of NSCLC. Our results show that EGFR targeting enhances tumor retention of SPIO nanoparticles. Further, magnetic hyperthermia treatment using targeted SPIO nanoparticles resulted in significant inhibition of *in vivo* lung tumor growth. Overall, this work demonstrates the potential for developing an effective anticancer treatment modality for the treatment of NSCLC based on targeted magnetic hyperthermia.

© 2013 Elsevier Ltd. All rights reserved.

1. Introduction

Despite earlier diagnosis and the availability of new molecularly-targeted drugs, lung cancer (specifically, non-small cell lung cancer; NSCLC) is still the leading cause of cancer-related deaths in the United States [1]. Surgical resection is the primary choice of treatment, followed by radiation and/or chemotherapy [2]. Metastatic and locally advanced disease stages are not amenable to surgical resection, and importantly, a majority of patients who undergo surgery eventually experience relapse [3–5]. Poor response rates and survival with current treatments clearly indicate the urgent need for developing an effective means to treat non-small cell lung cancer.

Magnetic hyperthermia is a novel non-invasive approach for tumor ablation and is based on heat generation by magnetic materials, such as superparamagnetic iron oxide (SPIO)

nanoparticles, when subjected to an alternating magnetic field (AMF) [6,7]. Depending on the size of SPIO nanoparticles and the frequency of AMF, heat is generated through either Néel or Brownian relaxation. The heat generated dissipates over short distances due to the high thermal conductivity of water and can, therefore, be used for highly focused heating [8,9]. However, inadequate delivery of magnetic nanoparticles to tumor cells can result in sub-lethal temperature change and induction of resistance [10]. Additionally, non-targeted delivery of these particles to the healthy tissues can result in heat damage to normal tissues.

In our studies, we developed epidermal growth factor receptor (EGFR)-targeted, inhalable SPIO nanoparticles for magnetic hyperthermia of non-small cell lung cancer (NSCLC). EGFR overexpression has been observed in as many as 70% of NSCLC patients [11–13], in whom EGFR expression is elevated in epithelial sites within tumors than in sites adjacent to and distant from tumors. We examined the effect of EGFR targeting on accumulation and retention of inhaled SPIO nanoparticles in the tumor tissue and the effect of targeted magnetic hyperthermia therapy on tumor growth in an orthotopic lung tumor model.

* Corresponding author. Department of Pharmaceutics, College of Pharmacy, University of Minnesota, Minneapolis, MN 55455, United States. Tel.: +1 612 624 0951; fax: +1 612 626 2125.

E-mail addresses: jpanyam@umn.edu, jpanyam@gmail.com (J. Panyam).

2. Materials and methods

2.1. Materials

Ferrous chloride tetrahydrate, ferric chloride hexahydrate, myristic acid, pluronic f127, ascorbic acid, potassium hydroxide, 1,10 phenanthroline and sodium acetate were purchased from Sigma (St. Louis, MO). Penicillin/streptomycin, fetal bovine serum, RPMI 1640, Dulbecco's phosphate buffered saline, F-12K (Kaighn's modification) and trypsin–EDTA solution were obtained from Invitrogen Corporation (Carlsbad, CA).

2.2. Synthesis of carboxy-terminated pluronic f127 (CTP)

The synthesis of CTP involved the use of an acid anhydride, which is highly susceptible to the presence of moisture. Hence, all the solvents used in the reaction were anhydrous and the reaction environment was maintained as dry as possible. A mass of 2 g of pluronic f127 was dissolved in 40 ml of anhydrous tetrahydrofuran. To the solution, 100 mg of 4-dimethylaminopyridine, 72 μ l of triethylamine and 800 mg of succinic anhydride were added, and the flask was sealed immediately. The mixture was stirred at room temperature for 48 h under nitrogen atmosphere. After 2 days, the volatile solvent was removed by rotary evaporation, and the dry residue was dissolved in 40 ml of carbon tetrachloride. The undissolved, unconjugated succinic anhydride was removed by filtration. The remaining polymer solution was concentrated using a rotary evaporator, and CTP was precipitated by drop-wise addition of the solution in cold, dry diethyl ether [14]. The residue was filtered, dried in a vacuum oven at 40 °C overnight and analyzed by proton NMR. The final yield of CTP was 1.74 g.

Completion of the reaction was confirmed by NMR. Around 25 mg of CTP was dissolved in 750 μ l of deuterated water and analyzed using a 400 MHz NMR. The NMR spectrum of unmodified pluronic f127 was also obtained for comparison.

2.3. Conjugation of EGFR-targeting peptide or the isotype scrambled peptide to CTP

A mass of 42 mg of CTP was dispersed in 1.8 ml deionized water. To this solution, 10 mg of *N*-(3-Dimethyl aminopropyl)-*N'*-ethylcarbodiimide hydrochloride (EDC) and 14 mg of *N*-hydroxysulfosuccinimide sodium salt (sulfo-NHS) (each dissolved in 100 μ l deionized water) were added and then stirred for 15 min at room temperature. The pH of the reaction mixture was 6–7. The excess unreacted EDC was quenched by the addition of β -mercaptoethanol at a final concentration of 130 mM. 10 mg of either the EGFR-targeted peptide (YHWYGYTPQNV1) or the scrambled peptide (HWPYAHPTHPSW) [15] was dissolved in 200 μ l of deionized water and added to the reaction mixture. 245 μ l of 10 \times PBS was added to buffer the reaction and the pH was maintained around 7–8. The reaction mixture was stirred overnight at room temperature [16]. The solution was dialyzed against water for 48 h using a 3500 Da molecular weight cutoff Slide-a-lyzer[®] dialysis cassette, and the final solution was lyophilized (Labconco, FreeZone 4.5, Kansas City, MO).

Conjugation of the peptides to CTP was confirmed by NMR. Around 25 mg of the conjugate was dissolved in 750 μ l of deuterated water and analyzed by a 400 MHz NMR. NMR spectra of the free peptides were used for identification of the resonances corresponding to the peptide.

2.4. Synthesis of water-dispersible SPIO nanoparticles

SPIO nanoparticles were synthesized from iron chlorides by the addition of a strong base, followed by coating with a fatty acid to prevent oxidation and then with a surfactant to form a stable aqueous dispersion [17]. Specifically, 0.82 g of ferric chloride hexahydrate and 0.33 g of ferrous chloride tetrahydrate were dissolved in 30 ml of degassed and nitrogen-purged water, and 3 ml of 5 M ammonium hydroxide was added drop-wise to this solution, which was then stirred for 30 min. The resulting iron oxide nanoparticles were washed three times with nitrogen-purged water, sonicated in a water-bath sonicator for 2 min, and then heated to 80 °C. About 100 mg of myristic acid was added to the heated mixture and stirred for another 30 min. Excess myristic acid was removed by two washes with ethanol, followed by two additional washes with water to remove excess ethanol. Each wash was followed by magnetic separation of nanoparticles. Myristic acid coated particles were then suspended in 30 ml water using a water-bath sonicator. Targeted or scrambled peptide conjugated pluronic, equivalent to 5% surface coverage of the peptide (5.5 mg and 11.7 mg of targeted and scrambled peptides, respectively), was mixed with pluronic f127 to yield a total mass of 100 mg, which was then added to the suspension and sonicated in a bath sonicator for 1 h. Every step of the synthesis was conducted carefully to minimize exposure to atmospheric oxygen.

2.5. Characterization of SPIO nanoparticles

The average hydrodynamic diameter of SPIO nanoparticles was determined by dynamic light scattering. About 1 mg of SPIO nanoparticles was dispersed in 2 ml of deionized water by sonication and the dispersion was subjected to particle size analysis using a Delsa[™] Nano C Particle Analyzer (Beckman, Brea, CA). The measurement was performed at 25 °C and at a 165° scattering angle. Mean

hydrodynamic diameter was calculated based on size distribution by weight, assuming a lognormal distribution. Five individual size measurement runs were performed, with each run recording 150 size events.

The iron content of the SPIO nanoparticles was measured using the 1,10 phenanthroline-based iron assay [18]. SPIO nanoparticles were first dissolved in 12 N hydrochloric acid. The solution was then diluted with distilled water to obtain a final acid concentration of 0.2 N. To the acid solution of SPIO nanoparticles, 10 mg/ml ascorbic acid, 1.2 mg/ml 1,10 phenanthroline, 22.4 mg/ml potassium hydroxide and 123 mg/ml sodium acetate were added in a volume ratio of 1:1:1:1:5. Absorbance of the resultant solution was measured at 490 nm using a microplate reader (Elx800 absorbance microplate reader, Biotek, Winooski, VT). Ferric chloride (hexahydrate) solution in 0.2 N hydrochloric acid was used as a standard.

2.6. Magnetic heating rate

SPIO nanoparticles were dispersed in 1 ml of Hank's F-12K medium in 10 mm \times 75 mm disposable borosilicate glass cell culture tubes. Magnetic heating was performed using an induction heating system (1 kW Hotshot, Ameritherm Inc., Scottsville, NY) by placing the suspension at the center of a multiturn copper coil that generated AMF (nominal magnetic field strength of 6 kA/m and frequency of 386 kHz). The temperature change was measured using a fluoroptic[®] probe (Lumasense Technologies, Santa Clara, CA) at five second intervals. Samples were equilibrated to 37 °C using a water-bath before exposure to the field.

2.7. Aerosol generation and characterization

Aerosolization of SPIO nanoparticles was achieved by ultrasonic atomization [19]. A Pyrex glass baffle was constructed in-house and placed in a water-bath, directly over a 1.7 MHz ultrasonic transducer [20]. About 13 ml of SPIO nanoparticle dispersion in 40% ethanol, containing 8 mg magnetite per milliliter was loaded into the baffle. Compressed air directed into the baffle at a flow rate of 0.5 L/min (as measured by an inline flow meter) entrained the aerosol droplets containing the SPIO nanoparticle dispersion and carried the particles into a subsequent drying assembly. The iron oxide output in the aerosol was measured by collecting the aerosolized and dried SPIO particles for a predetermined period of time on Whatman quartz microfiber filters suitable for air sampling [21]. The filters were assayed using the above procedure and the iron oxide output rate was calculated as iron oxide amount collected per unit time.

The aerosol particle size distribution was determined with a Mercer style seven-stage Intox cascade impactor operating at a sample flow rate of 0.5 L/min. The aerosol generated was passed through a heated drying column before passing through the cascade impactor. Aerosol particles deposited at each stage of the cascade impactor were collected and analyzed by iron assay to obtain the particle size distribution. The mass median aerodynamic diameter (MMAD) and associated geometric standard deviation (GSD) were calculated from linear regression of an X-probability plot of the cumulative undersized mass as a function of logarithm of the impactor stage cutoff diameter using OriginPro 8 software (OriginLab Corporation, Northampton, MA) [21].

2.8. Cell culture studies

A549 (human lung adenocarcinoma) and A549-luc (luciferase-transfected A549) cells were used in the study. Both cell lines were propagated using F-12K medium supplemented with 10% fetal bovine serum (FBS) and 1% antibiotic solution and maintained at 37 °C and in 5% carbon dioxide.

2.8.1. Demonstration of role of EGFR in tumor cell uptake of functionalized nanoparticles

A549 cells were plated in a 6-well plate 4 h before the start of the study. Cells were washed with phosphate buffered saline (PBS) to remove non-adherent cells and 1 mg (magnetite equivalent) of targeted SPIO particles, scrambled peptide-conjugated particles, particles without any peptide, or targeted particles with excess free targeting peptide were added to the cells in a total volume of 2 ml of cell culture medium containing 5% FBS. The plates were incubated on ice for 30 min, washed thrice with PBS and incubated at 37 °C for an additional 45 min. At the end of the incubation, cells were lysed with 400 μ l of RIPA buffer and assayed for total cell protein content and iron content [18] (by iron assay procedure described before).

To evaluate EGFR targeting on the effectiveness of magnetic hyperthermia, plated A549 cells were incubated with targeted or non-targeted particles for 30 min at 4 °C, washed three times with PBS, incubated at 37 °C for 45 min and then subjected to AMF (6 kA/m at 386 kHz frequency). Following AMF exposure, 10 μ M propidium iodide was added to the cells and observed under a fluorescent microscope immediately and at 24 h after AMF exposure.

2.9. Orthotopic lung tumor model

All animal studies were carried out in compliance with protocol approved by the Institutional Animal Care and Use Committee at the University of Minnesota. Female

Fox Chase SCID[®] Beige mice (CB17.Cg-Prkd^{scid}Lyst^{bg-j}/Cr1) 4–5 weeks of age, were obtained from Charles River Laboratories.

A mouse orthotopic lung tumor model [22] was used in the studies. Lung tumor cells that have been stably transfected with firefly luciferase were used to facilitate the visualization of tumor cells in live animals using bioluminescence imaging. A549-luc-C8 Bioware[®] Cell Line (Caliper Lifesciences) is a luciferase expressing cell line derived from A549 human lung squamous carcinoma cells by stable transfection of the North American Firefly Luciferase gene expressed from the CMV promoter. Intravenous injection of 1×10^6 A549-luc-C8 cells led to detectable increase in bioluminescence in the lungs by 2 weeks.

2.10. Lung delivery of SPIO nanoparticles

2.10.1. Tracheal instillation

The mice were anesthetized and placed on a rodent intubation stand, supported by their incisors. The tongue was rolled out using a sterile cotton swab and held between the fingers. A fiber-optic light and stylus (BioLite, BioTex, Inc., TX) connected to an endotracheal tube was used to visualize the tracheal opening and to carefully insert the attached endotracheal tube into the trachea. An inflation bulb was used to confirm the proper insertion of the endotracheal tube by monitoring the inflation of the thoracic region on gently pushing in air through the tube. Targeted or non-targeted SPIO particles (50 μ l, 10 mg/ml iron oxide equivalent) were instilled through the endotracheal tube. The mice were kept upright for a minute to prevent back-flow of the liquid and then placed on a heating pad to assist in faster recovery from anesthesia [23].

2.10.2. Inhalation

The aerosol was generated as described above, but the dried SPIO aerosols were directed through the drying assembly into an animal chamber, which comprised a 4-port double-walled chamber. The dried aerosol stream entered the top inlet into a stirred chamber. The animals were placed into each port with their nose exposed to the aerosol stream in the stirred chamber. The exhaust tube was connected to the space between the two walls, thus ensuring that the mice underwent a “nose-only” exposure for 30 min. Filter collections were made three times both before and after the exposure to measure the aerosol output. The aerosol stream was also passed through a seven-stage Intox cascade impactor before each exposure to determine the aerosol particle size distribution (MMAD and GSD) [21].

2.11. Distribution of SPIO nanoparticles following instillation and inhalation delivery

Targeted or scrambled peptide conjugated SPIO nanoparticles were administered to tumor-bearing animals ($n = 6$ per time point per group) by the two routes of administration described above. The animals were euthanized at 1 h, 1 day or 1 week after SPIO administration. The lungs, liver, spleen, kidney, heart, stomach and blood were collected to analyze the distribution of SPIO particles. Additionally, lungs of treated animals were also sectioned, stained with hematoxylin and eosin (H&E staining) and Prussian blue (for iron) [24] and imaged after the last time point to visualize the distribution of SPIO particles. Basal level of iron in each organ was determined in six healthy mice and subtracted from the assayed iron content in the treatment groups. The difference was used to determine the contribution of SPIO nanoparticle administration to tissue iron concentrations.

2.12. In vivo efficacy of targeted magnetic hyperthermia after inhalation delivery of SPIO nanoparticles

Fox Chase SCID[®] Beige mice were injected with A549-luc cells intravenously to facilitate the development of tumors in the lungs. Once the lung bioluminescence reached about 0.5×10^6 photons/s, animals were administered SPIO nanoparticles by inhalation. After 7 days, some of the treated animals were subjected to 30 min of magnetic hyperthermia. Untreated animals and animals receiving the particles without exposure to AMF served as controls. Lung bioluminescence was monitored three times weekly for 4 weeks. At the end of the study, animals were euthanized, and the lungs and trachea were removed and weighed. Assuming little variability between the lung weights of individual mice, the differences in lung weights were attributed to the variable mass of lung tumors.

2.13. Statistical analysis

Statistical analyses were performed using one-way ANOVA, followed by Bonferroni–Holm method for comparison between individual groups. A probability level of $P < 0.05$ was considered significant.

3. Results

3.1. Characterization of inhalable SPIO nanoparticles

Conversion of the hydroxyl end group of pluronic f127 into a carboxyl group was confirmed using NMR spectroscopy and the

conversion efficiency was almost 100% (Fig. 1a and b). Presence of targeted or scrambled peptides could be detected in the NMR spectra of the modified polymer (Fig. 1c–f). The conjugation efficiency of EGFR-targeted peptide and scrambled peptide to CTP was $90.4 \pm 10.5\%$ and $42.8 \pm 4.6\%$ respectively. SPIO nanoparticles were composed of $74 \pm 2\%$ w/w iron oxide, coated with $10 \pm 3\%$ w/w myristic acid, and stabilized by $16 \pm 2\%$ w/w pluronic f127. The hydrodynamic diameter of unconjugated (pluronic COOH terminated) SPIO nanoparticles was 309 ± 24 nm while that of targeted peptide and scrambled peptide-conjugated particles was 369 ± 34 nm and 365 ± 45 nm, respectively. The heating rate of SPIO nanoparticles was concentration-dependent, and was similar for both targeted and non-targeted SPIO nanoparticles (Fig. 1g).

3.2. In vitro cell uptake and cell kill efficiency of targeted SPIO nanoparticles

Non-specific uptake of SPIO nanoparticles in A549 cells was determined as a function of time of incubation, concentration of serum in the culture medium and the incubation temperature. From these studies, an incubation time of 30 min and low serum concentration were found to be optimal for minimizing the non-specific uptake of SPIO nanoparticles. Using these optimized parameters, an *in vitro* study was performed to determine the effect of EGFR targeting on cellular uptake of SPIO nanoparticles. Nanoparticle uptake into cells was 4.5-fold higher for the EGFR-targeted formulation than that for the non-targeted control. Conjugation of scrambled peptide did not result in enhancement of particle uptake into cells, and the presence of excess targeting ligand decreased the cellular uptake of targeted nanoparticles, showing the specific role of EGFR in tumor cell uptake of targeted nanoparticles (Fig. 2a). Some of the experimental conditions (low serum, initial 4 °C, low incubation time) used in this assay are not representative of physiological conditions. However, the goal here was to demonstrate that targeted particles bind to the tumor cells to a higher extent relative to non-targeted particles. The parameters used here facilitated binding of particles to cells while minimizing non-specific uptake.

To determine the effect of EGFR targeting on the effectiveness of magnetic hyperthermia, plated A549 cells were incubated with targeted or non-targeted SPIO nanoparticles, washed and subjected to AMF. Enhanced cellular accumulation of EGFR-targeted SPIO nanoparticles could be visualized under the microscope as dark spots on the cells (Fig. 2e and f). Magnetic hyperthermia with targeted nanoparticles resulted in greater number of cells taking up propidium iodide, indicating enhanced cell death with targeted SPIO nanoparticles (Fig. 2b–f).

3.3. In vivo lung deposition and retention after inhalation delivery

Ultrasonic atomization of SPIO nanoparticle dispersions resulted in aerosols with a MMAD of 1.1 ± 0.1 μ m and GSD of 1.9 ± 0.1 (Supp. Inf. 1). The iron oxide output rate was determined to be 270 ± 70 μ g/min. The high iron oxide output and the MMAD size range point to the possibility of a high deposition of these aerosol particles in the mouse lung even with a relatively short exposure time.

Following aerosol exposure, iron oxide concentration in the lungs at 1 h (Fig. 3a) was similar for targeted and non-targeted SPIO nanoparticles in tumor-bearing lungs as well as for blank SPIO particles in healthy lungs, showing that the presence of tumor did not affect the total deposition of particles. It also suggested that targeting does not affect the lung concentration immediately after the administration of particles. However, 1 week following inhalation, the lung concentration of non-targeted particles decreased

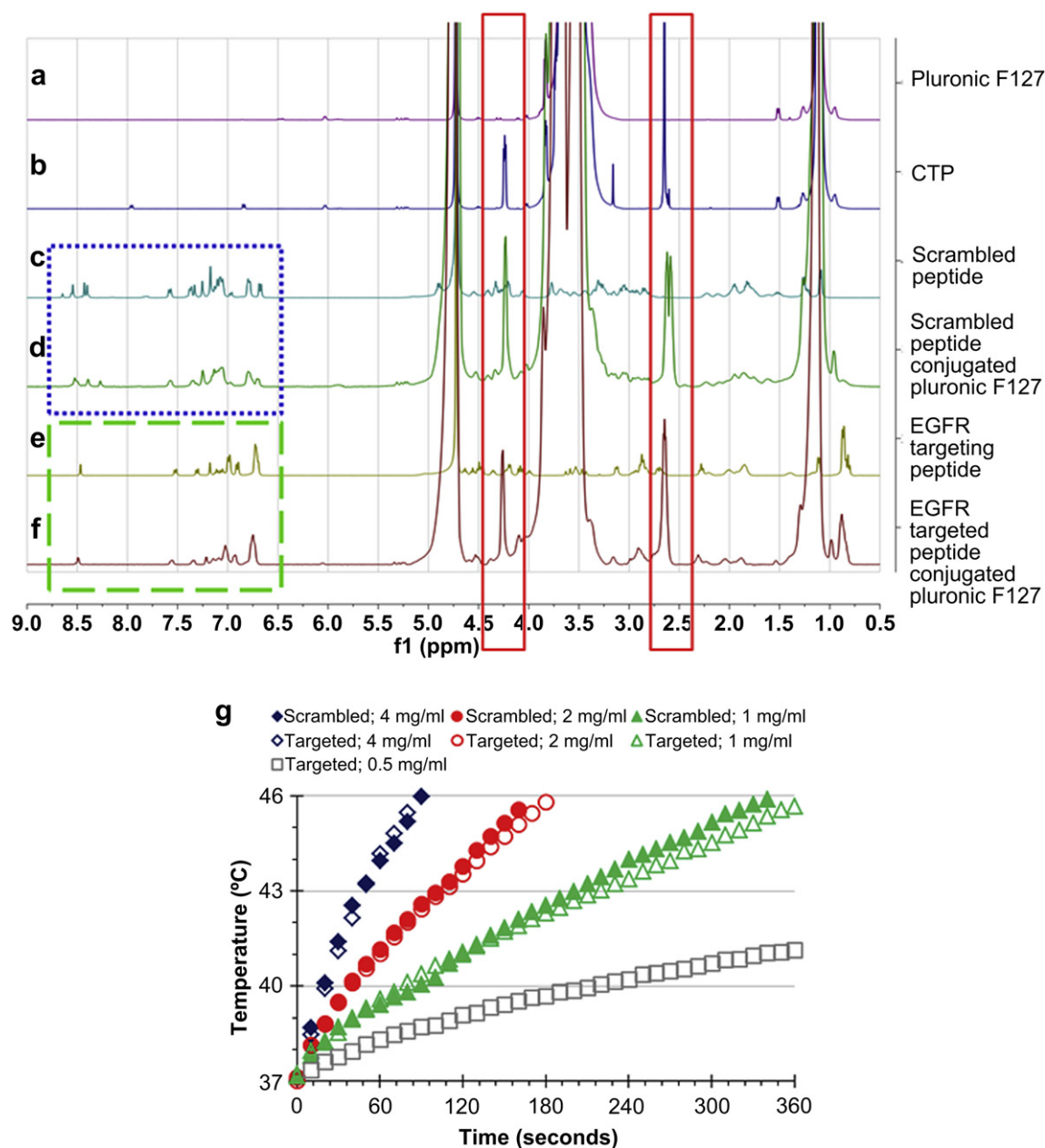


Fig. 1. SPIO NP formulation and characterization. (a–f) NMR spectra of modified pluronic f127. (a) Pluronic f127 has a characteristic NMR peak at 1.02 ppm and multiple peaks between 3 and 4 ppm. (b) Conjugation of carboxy end group can be detected by the appearance of new peaks at 2.6 and around 4.2 ppm (solid box). NMR spectrum of (e) EGFR-targeting peptide is different from (c) scrambled peptide with the most visible difference between 6 and 9 ppm. Peptide conjugation to the carboxy-terminated pluronic (CTP) can be verified from the presence of both carboxy modification peaks (solid box) and (f) EGFR-targeting peptide (dotted box) or (d) scrambled peptide (dashed box) peaks. (g) **Heating rates of targeted and non-targeted SPIO nanoparticles.** SPIO nanoparticle dispersions were placed in an alternating magnetic field of 6 kA/m and operating at a frequency of 386 kHz. The initial temperature was equilibrated to 37 °C, and the temperature of SPIO NP dispersion was measured at 10 s intervals using a fluoroptic probe.

while the level of targeted particles was almost constant, demonstrating the effectiveness of EGFR targeting in improving particle retention within tumor-bearing lungs.

Inhalation delivery resulted in a homogenous distribution of SPIO nanoparticles throughout the lung (Fig. 3b and c). One week after inhalation, a significantly higher amount of Prussian blue staining was observed in the mice that received targeted particles compared to those that received non-targeted particles. In the former, the staining was observed in and around tumor cells (Fig. 3d and e), with near complete absence of particles from the healthy parts of the lung. In contrast, the latter group did not display much staining in either the tumor or the healthy regions of the lung (not shown).

3.4. Biodistribution of SPIO nanoparticles after high dose instillation into lungs

To study the effect of elevated lung dose of SPIO nanoparticles on the overall body distribution, we used tracheal instillation. Unlike inhalation delivery, which restricts the dose deposited in mouse lungs to $72.5 \pm 14.1 \mu\text{g}$ of magnetite, tracheal instillation allows for a higher dose ($386 \pm 95 \mu\text{g}$ of magnetite) to be delivered.

Following instillation, SPIO particles were mostly observed in the lungs after 1 h, although some particles were also present in the stomach, due to the mucociliary clearance from the lung. There was no significant difference between the levels of targeted and non-targeted particles in the different organs 1 h or 1 day after

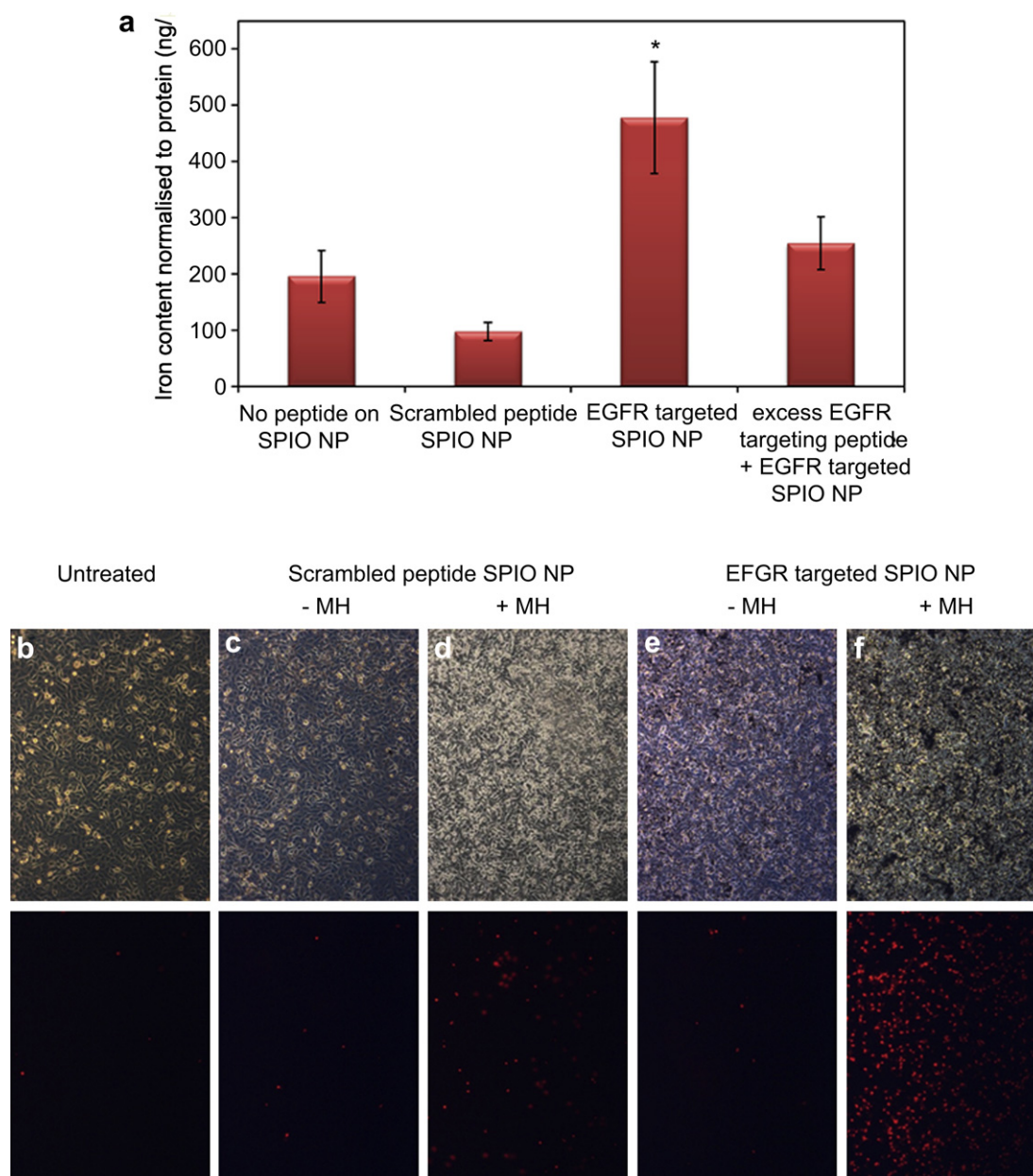


Fig. 2. *In vitro* cell uptake (a) and cell kill efficacy (b–f) of EGFR-targeted SPIO nanoparticles. (a) SPIO nanoparticles bearing EGFR-targeting peptide, scrambled peptide or no peptide on the surface were incubated with A549 cells at 4 °C for 30 min, washed with PBS and further incubated at 37 °C for 45 min. The specific role of EGFR in enhanced accumulation was determined by adding excess EGFR-targeting peptide to competitively inhibit the binding of targeted SPIO nanoparticles. Iron content of the lysed cells was used to calculate the cellular uptake of SPIO nanoparticles. $n = 3$. * $P < 0.05$ compared to other controls. (b–f) A549 cells were incubated with (b) culture medium, (c and d) non-targeted or (e and f) targeted SPIO nanoparticles and subjected to magnetic hyperthermia (MH) for 30 min (d and f). PI was added immediately before MH treatment. The top panel shows the phase contrast microscopic images, while the bottom panel shows the corresponding fluorescent microscopic images of PI positive cells.

instillation. The concentration of both particles in blood and other organs (except lung) decreased 1 week after instillation compared to 1 h or 1 day time points (Fig. 4a and b). On the contrary, while the lung concentration of non-targeted particles decreased over the period of 1 week, the level of targeted particles was fairly constant over 1 week. The final concentration of targeted particles was significantly higher (60%) than non-targeted particles 1-week post-instillation (Fig. 4c). In contrast to the high lung concentration, the amount of iron in the other tissues was virtually unchanged throughout the duration of the study and was not considerably different from the basal level of iron in the tissues of untreated animals (Fig. 4d). This data suggested that pulmonary delivery of

targeted SPIO nanoparticles can circumvent non-specific distribution into organs such as liver and spleen, which commonly receive the highest dose of intravenously administered therapeutics [25].

While both instillation and inhalation resulted in a significant increase in lung concentration of particles with EGFR targeting, the absolute amount of SPIO particles in the two cases were different. The lung iron content after instillation was 4.5–5-fold higher than that after inhalation (400 vs 80 μg for EGFR-targeted SPIO nanoparticles, Figs. 3 and 4). This is likely due to the higher dose of particles delivered to the lung through instillation. However, aerosol delivery is a more convenient route of administration in humans than instillation. Additionally, inhalation resulted in a

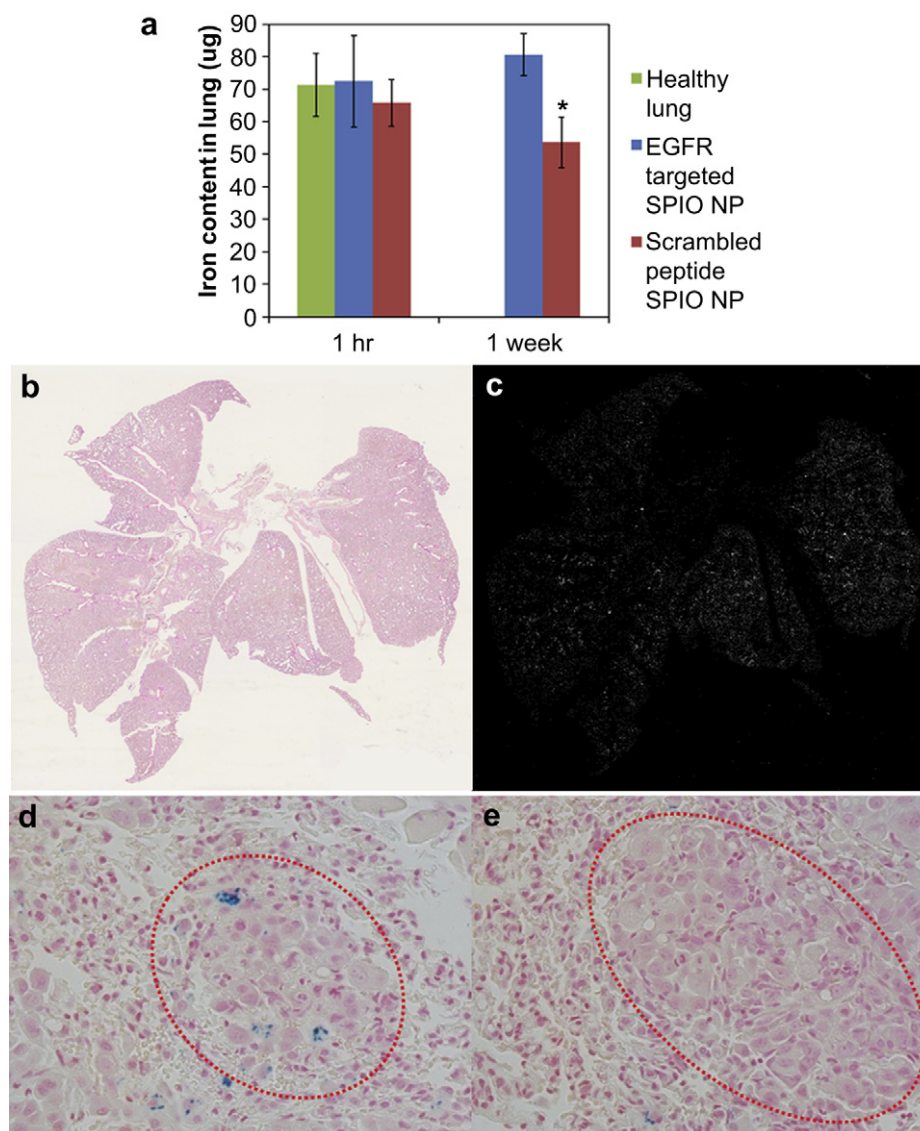


Fig. 3. (a) *In vivo* lung deposition and retention of SPIO nanoparticles after inhalation delivery. Healthy mice or those bearing orthotopic A549 tumors were allowed to inhale targeted or non-targeted SPIO nanoparticles for 30 min. Animals were euthanized 1 h or 1 week after inhalation delivery and the lungs were assayed for iron content ($n = 4$; $*P < 0.01$ compared to non-targeted group at 1 week after inhalation). (b and c) **Distribution of SPIO nanoparticles in mouse lung after inhalation.** One hour after inhalation of SPIO nanoparticles, animals were euthanized, lungs were collected, sectioned and stained with Prussian blue. Due to the difficulty in visualizing Prussian blue staining of the entire mouse lung (b), an image processing software (Image Pro Plus) was used to pseudo-color the Prussian blue stain white against a black background (c). (d and e) **Prussian blue staining of lung tumor section after SPIO nanoparticle inhalation.** One week after inhalation of targeted (d) or non-targeted SPIO nanoparticles (e), mice were euthanized, lungs were collected, sectioned and stained with Prussian blue. The sections show the presence of SPIO nanoparticles in tumor nodules (marked by red ovals) in EGFR-targeted group (100 \times magnification).

more even distribution of the SPIO nanoparticles throughout the lungs at the time of administration (Fig. 3a) compared to instillation, where most of the instilled dose resided near the major airways, with almost no particles reaching the periphery (Supp. Inf. 2).

3.5. *In vivo* efficacy after inhalation

Magnetic hyperthermia using non-targeted SPIO particles resulted in an insignificant decrease in lung tumor bioluminescence ($P > 0.05$) relative to that in animals that received the same particles but were not exposed to AMF. Targeted SPIO nanoparticles mediated hyperthermia showed significantly lower lung tumor bioluminescence ($P < 0.05$) (Fig. 5a). The lung weights at the end of the study agreed with the bioluminescence data; magnetic

hyperthermia with targeted particles resulted in a significantly lower final lung weight compared to the other groups (Fig. 5b).

These *in vivo* results thus confirm that EGFR targeting enhances the tumor concentration of SPIO nanoparticles, which translated into more effective tumor cell kill. In addition, the treated mice showed no signs of distress over the duration of the study (30 days after magnetic hyperthermia treatment), suggesting that this procedure does not result in acute systemic toxicity or damage to healthy lung tissue. Additionally, the dose of particles that could be delivered to the tumor by inhalation was limited by the small lung volume and the obligate nose-breathing of mice [26]. A similar approach can be expected to be more effective in humans, because a higher deposition can be achieved with inhalation through the oral cavity and control of the respiration.

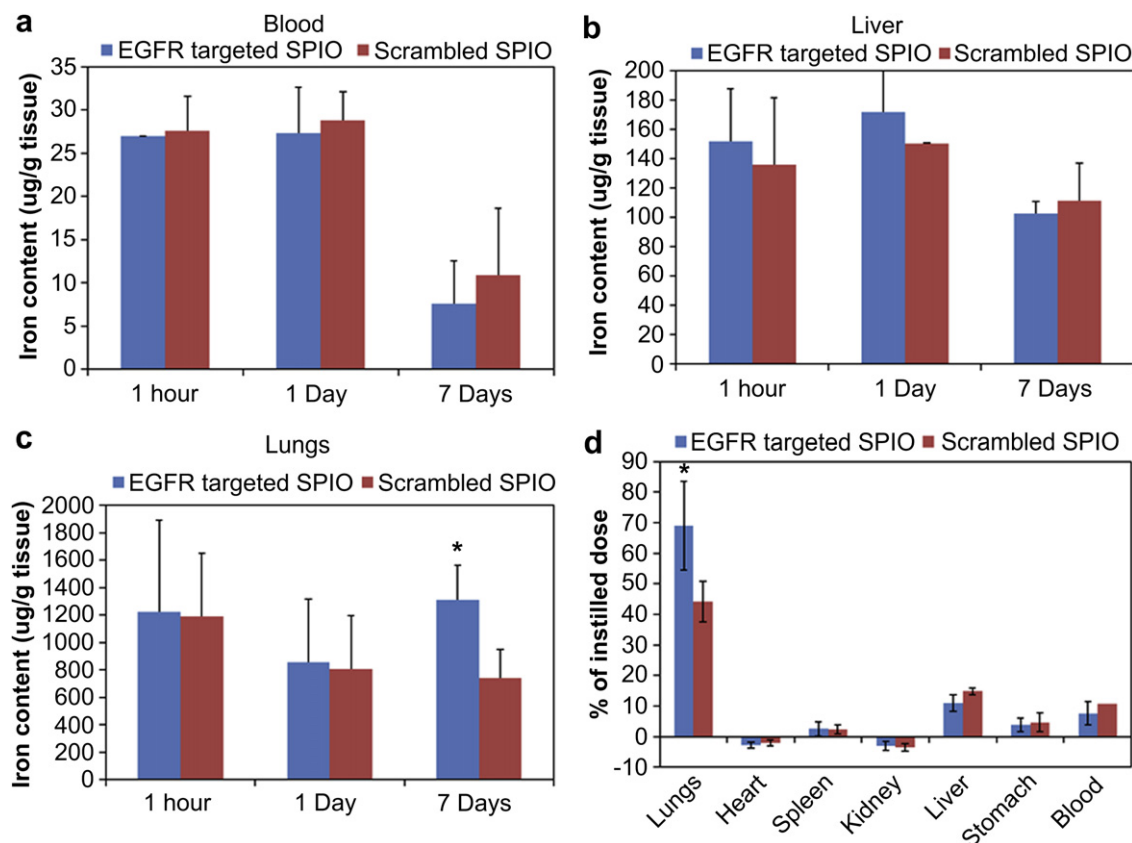


Fig. 4. (a–c) Iron content in different tissues after SPIO nanoparticle instillation. Iron content in (a) blood, (b) liver and (c) lung after 1 h, 1 day or 1 week after instillation of targeted or non-targeted SPIO nanoparticles. Iron concentration remained elevated in blood and liver for 24 h after instillation and decreased after a week. There was no significant effect of targeting on the iron levels in blood and liver ($n = 4$). In contrast, EGFR targeting enhanced lung retention of SPIO nanoparticles over a week ($n = 4$; $*P < 0.05$ compared to non-targeted group at 1 week after instillation). (d) Distribution of SPIO nanoparticles 1 week post-instillation. Iron content in lungs, heart, spleen, kidneys, liver, stomach and blood are shown as a percent of instilled dose. Overall levels of iron in the organs were low except for the lungs ($n = 4$; $*P < 0.05$ compared to non-targeted group at 1 week after instillation).

4. Discussion

Magnetic hyperthermia, which involves the use of superparamagnetic substances to generate heat through application of an external AMF, is a non-invasive approach for lung tumor ablation. The relatively inert nature of the magnetic substances in the absence of magnetic field and their efficacy in the presence of AMF make this technique highly suitable for achieving an on-demand response. Magnetic hyperthermia is particularly suitable for the treatment of lung cancer since unlike the abdomen, the thoracic region, where the external AMF can be easily focused, is only inhabited by the lungs and the heart. Additionally, lungs are filled with air, which act as a poor conductor of heat. Thus, the heat generated by the particles in the lungs is less likely to affect the surrounding organs such as the heart. Finally, studies have shown that normal, non-malignant cells are more resilient to heat damage than tumor cells [27], thereby minimizing the chances of damage to healthy lung tissue. Recent reports have suggested that magnetic hyperthermia is effective in murine subcutaneous lung tumor models [28,29]. However, in spite of the promise of a highly effective treatment option, no studies have so far assessed the effectiveness of magnetic hyperthermia in an orthotopic lung tumor model.

Although the lung is a highly perfused organ, intravenous delivery of anticancer therapeutics targeted to the lung results in broad, non-specific distribution of the therapeutic agents to normal organs, resulting in severe systemic side effects [30]. While many

solid tumors are not amenable to local delivery, lung tumors of the epithelial origin can potentially be accessed by inhalation route. This allows for maximizing the concentration of the therapeutic agent in the target organ, i.e., the lungs, while minimizing exposure to other normal organs. Lung clearance of particulates into systemic circulation is primarily attributed to the alveolar macrophages, which leads to a lower blood concentration of the therapeutics than through intravenous administration. Several reports have shown that pulmonary delivery improves retention of therapeutic agents in the lungs while limiting their concentration in the blood thereby reducing their levels in the healthy organs [25,31]. Our studies show that lung delivery through either instillation or inhalation results in therapeutically effective concentrations of SPIO nanoparticles in lungs with minimal exposure to other organs. An hour after instillation of SPIO nanoparticles, the average lung concentration of iron oxide was 1.2 mg/g of tissue. In contrast, the average liver and blood concentration were 130 $\mu\text{g/g}$ and 27 $\mu\text{g/g}$ of tissue, respectively. The other organs including spleen, kidney and heart contained less than 2% of the instilled dose. This demonstrates that inhalation delivery is an effective means to enhance local concentration of therapeutics into the lungs.

It was interesting to note that the iron concentration in blood was high at 1 h and 1 day, but then decreased at 7 days after tracheal instillation. There are two possible explanations for this observed result. First, despite careful dosing into the trachea, a part of the instilled dose could get regurgitated and swallowed by the animals. The SPIO particles in the stomach can dissolve in the

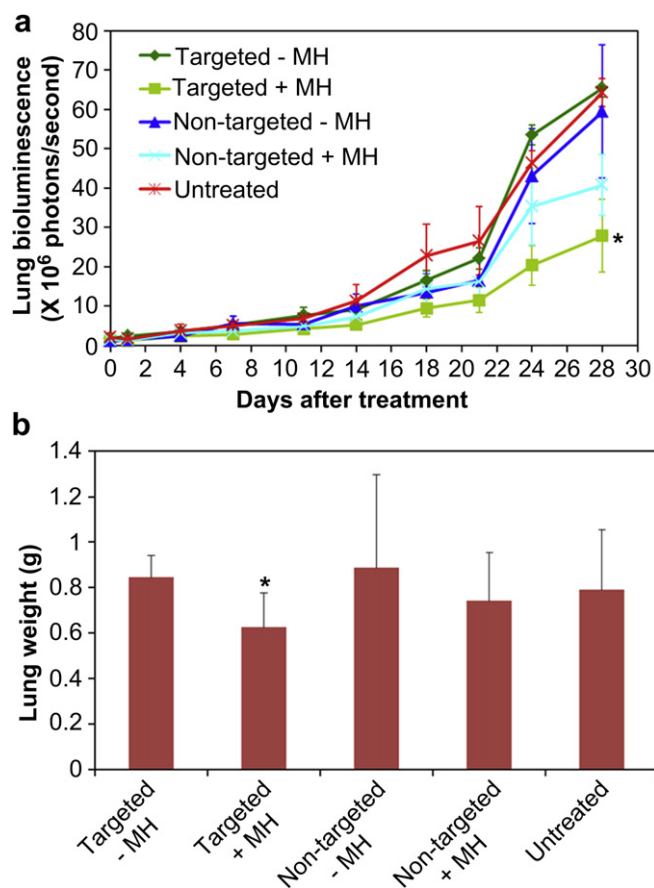


Fig. 5. Effect of targeted magnetic hyperthermia on lung tumor growth. Orthotopic lung tumor-bearing mice were allowed to inhale targeted or non-targeted SPIO nanoparticles. After 1 week, 6 animals from each group were subjected to magnetic hyperthermia (MH) for 30 min. (a) Lung tumor bioluminescence was monitored over a period of 1 month. Data shown as mean \pm SD ($n = 6$; * $P < 0.05$ compared to saline-treated and unheated controls). (b) Lungs were collected at the end of the efficacy study (1 month after magnetic hyperthermia) and weighed. Data shown as mean \pm SD ($n = 6$; * $P < 0.05$ compared to unheated control).

highly acidic gastric pH to form soluble iron salts, which are then absorbed into the blood stream. This will lead to high initial iron content in the blood. This soluble iron can be cleared from blood relatively easily, resulting in a decrease in the iron levels after a week. Second, immediately after instillation, SPIO nanoparticles in the lung are free and can be absorbed into the blood stream. However, at later time points, particles are likely internalized into the tumor cells (and/or macrophages) and hence not readily available for absorption. This would also result in high initial iron concentration in the blood, followed by a drop at later times.

Following inhalation delivery, it is expected that nanoparticles would be distributed to both the malignant and healthy regions of the lungs. The presence of targeting ligand on the surface is expected to enable nanoparticles to bind to the tumor cells, allowing for greater retention in the tumor tissue. Thus, greater retention within the tumor tissue and clearance from normal tissue are expected to eventually result in relatively higher levels of nanoparticles in the tumor. Application of AMF during this window would allow for tumor-specific induction of hyperthermia. In our studies, tumor cell specificity was achieved by targeting SPIO nanoparticles to EGFR, which is overexpressed in NSCLC tumors [11–13]. Monoclonal antibodies against EGFR (cetuximab) and EGFR tyrosine kinase inhibitors are clinically used for lung cancer. Thus, EGFR is an attractive target in lung cancer. We used a

previously reported 11-residue peptide ligand for targeting EGFR [15]. This peptide binds specifically and efficiently to EGFR (dissociation constant of ~ 20 nM), but has much lower mitogenic activity than EGF [15]. We found that EGFR targeting enhanced the *in vitro* accumulation of targeted SPIO nanoparticles into A549 cells by 450% compared to non-targeted particles. Aerosolized SPIO particles were directed to the periphery of the lung by controlling the aerodynamic size of SPIO aggregates. One hour after inhalation, the amount of the targeted or non-targeted particles was similar in tumor-bearing or healthy lungs (about 70 μg iron oxide). However, following mucociliary clearance from the lung (1 week after inhalation delivery), the level of non-targeted SPIO nanoparticles was significantly lower than that of targeted particles. This difference could be attributed to the presence of tumor targeting ligand on the surface. Thus, by combining receptor targeting with inhalation delivery, superior tumor selectivity can be achieved.

There are several challenges in the design of an effective inhalation system, which can deposit a high dose to the peripheral regions of the lung. Mice are obligatory nose breathers, with a small inhalation volume (~ 24.5 ml/min). This restricts the rate of delivery of therapeutics into the lungs. The dose delivered can, however, be controlled by changing the concentration of the aerosol generated (mass of aerosol/volume of air) and the aerodynamic diameter of the aerosol. An MMAD of 1 μm has been shown to result in the highest concentration of the therapeutic agents in all lobes of mouse lungs [32], yielding a deposition percent (ratio of mass deposited in the lungs to total mass inhaled) of about 10% [21,33]. In our studies, we obtained a deposition of nearly 15% with the 1.1 μm MMAD SPIO nanoparticles. The elevated deposition fraction was probably attributed to pre-acclimatization of the mice to the inhalation chambers and the prolonged exposure (30 min), which prevented undue stress and uneven breathing pattern caused by short aerosol exposures. This fraction is amenable to further enhancement by using magnetic deposition [21] or micro-spraying technique [34], which can increase the deposition fraction of SPIO nanoparticles by several folds.

The effectiveness of targeted magnetic hyperthermia was evaluated in an orthotopic mouse lung tumor model. Intravenous injection of A549 cells led to the development of lung tumors, whose bioluminescence scaled with the size of the tumor. Lung tumors could be identified at a bioluminescence level of 1×10^5 photons/s and the tumor burden reached 90% of the lung volume at 5×10^8 photons/s. Using an optimized aerosol formulation of targeted SPIO nanoparticles, we could achieve therapeutic doses of SPIO nanoparticles in the tumors. A single magnetic hyperthermia regimen was effective in reducing the tumor growth rate over a month compared to the non-targeted or non-treated control. In addition, the treatment did not result in any toxic manifestations in the mice.

Due to their epithelial nature, lung tumors fill up the alveolar region and thus, most tumors are not exposed to the circulating airways. This poses a challenge to the success of the nanoparticle system. In spite of enhanced retention of targeted SPIO nanoparticles in the tumor, not all tumor cells possessed particles and therefore would not receive magnetic hyperthermia therapy. As a result, the treatment showed a significant delay in tumor growth but not complete eradication. However, this problem could potentially be addressed by using agents that normalize the tumor extracellular matrix and enhance the penetration of nanoparticles into the tumor [35,36]. Additionally, SPIO nanoparticle mediated magnetic hyperthermia may be highly effective as an adjuvant therapy for killing isolated tumors cells left behind after surgical resection of the lung tumors.

5. Conclusions

Inhalation delivery of EGFR-targeted SPIO nanoparticles was investigated in this study as a potential approach for lung cancer treatment. Our studies show that EGFR targeting enhances tumor retention of SPIO nanoparticles while minimizing systemic exposure. Tracheal instillation allowed for high doses of SPIO nanoparticles to be administered, however, aerosol delivery resulted in better intra-tumoral distribution. Magnetic hyperthermia using targeted SPIO nanoparticles resulted in a significant inhibition of *in vivo* tumor growth. Overall this work highlights the potential for developing magnetic hyperthermia as an effective anticancer treatment modality for the treatment of non-small cell lung cancer.

Acknowledgments

Parts of this work were carried out in the Characterization Facility, University of Minnesota, which receives partial support from NSF through the MRSEC program. We also thank the Comparative Pathology core facility for the preparation of H&E and Prussian blue stained slides.

We thank Ying Jing (Electrical and Computer Engineering, University of Minnesota) for help with magnetization studies, Paula Overn (Comparative Pathology, University of Minnesota) for the preparation of histopathology slides and Brenda Koniar (Research Animal Resources, University of Minnesota) for assistance with animal studies.

Funding support from the Department of Defense (CA093453).

Appendix. Supplementary data

Supplementary data related to this article can be found online at <http://dx.doi.org/10.1016/j.biomaterials.2013.03.061>.

References

- [1] Cancer trends progress report – 2012 update. Bethesda, MD: National Cancer Institute, NIH, DHHS; 2012.
- [2] Non-small cell lung cancer treatment (PDQ®). Available from: <http://www.cancer.gov/cancertopics/pdq/treatment/non-small-cell-lung/patient>.
- [3] Shaw EG, Brindle JS, Creagan ET, Foote RL, Trastek VF, Buskirk SJ. Locally recurrent non-small-cell lung cancer after complete surgical resection. *Mayo Clin Proc* 1992;67(12):1129–33.
- [4] Kelsey CR, Marks LB, Hollis D, Hubbs JL, Ready NE, D'Amico TA, et al. Local recurrence after surgery for early stage lung cancer: an 11-year experience with 975 patients. *Cancer* 2009;115(22):5218–27.
- [5] Thomas P, Rubinstein L. Cancer recurrence after resection: T1 N0 non-small cell lung cancer. Lung Cancer Study Group. *Ann Thorac Surg* 1990;49(2):242–6.
- [6] Hiergeist R, Andrä W, Buske N, Hergt R, Hilger I, Richter U, et al. Application of magnetite ferrofluids for hyperthermia. *J Magn Magn Mater* 1999;201(1–3):420–2.
- [7] Jordan A, Scholz R, Wust P, Fähling H, Roland F. Magnetic fluid hyperthermia (MFH): cancer treatment with AC magnetic field induced excitation of biocompatible superparamagnetic nanoparticles. *J Magn Magn Mater* 1999;201(1–3):413–9.
- [8] Tasci TO, Vargel I, Arat A, Guzel E, Korkusuz P, Atalar E. Focused RF hyperthermia using magnetic fluids. *Med Phys* 2009;36(5):1906–12.
- [9] Tseng HY, Lee GB, Lee CY, Shih YH, Lin XZ. Localised heating of tumours utilising injectable magnetic nanoparticles for hyperthermia cancer therapy. *IET Nanobiotechnol* 2009;3(2):46–54.
- [10] Jung H. Interaction of thermotolerance and thermosensitization induced in CHO cells by combined hyperthermic treatments at 40 and 43 degrees C. *Radiat Res* 1982;91(3):433–46.
- [11] Merrick DT, Kittelson J, Winterhalder R, Kotantoulas G, Ingeberg S, Keith RL, et al. Analysis of c-ErbB1/epidermal growth factor receptor and c-ErbB2/HER-2 expression in bronchial dysplasia: evaluation of potential targets for chemoprevention of lung cancer. *Clin Cancer Res* 2006;12(7 Pt 1):2281–8.
- [12] Tang X, Varella-Garcia M, Xavier AC, Massarelli E, Ozburn N, Moran C, et al. Epidermal growth factor receptor abnormalities in the pathogenesis and progression of lung adenocarcinomas. *Cancer Prev Res* 2008;1(3):192–200.
- [13] Varella-Garcia M, Mitsudomi T, Yatabe Y, Kosaka T, Nakajima E, Xavier AC, et al. EGFR and HER2 genomic gain in recurrent non-small cell lung cancer after surgery: impact on outcome to treatment with gefitinib and association with EGFR and KRAS mutations in a Japanese cohort. *J Thorac Oncol* 2009;4(3):318–25.
- [14] Chittasupho C, Xie SX, Baum A, Yakovleva T, Siahaan TJ, Berkland CJ. ICAM-1 targeting of doxorubicin-loaded PLGA nanoparticles to lung epithelial cells. *Eur J Pharm Sci* 2009;37(2):141–50.
- [15] Li Z, Zhao R, Wu X, Sun Y, Yao M, Li J, et al. Identification and characterization of a novel peptide ligand of epidermal growth factor receptor for targeted delivery of therapeutics. *FASEB J* 2005;19(14):1978–85.
- [16] Grabarek Z, Gergely J. Zero-length crosslinking procedure with the use of active esters. *Anal Biochem* 1990;185(1):131–5.
- [17] Jain TK, Morales MA, Sahoo SK, Leslie-Pelecky DL, Labhasetwar V. Iron oxide nanoparticles for sustained delivery of anticancer agents. *Mol Pharmacol* 2005;2(3):194–205.
- [18] Krishna Murti GSR, Moharir AV, Sarma VAK. Spectrophotometric determination of iron with orthophenanthroline. *Microchem J* 1970;15(4):585–9.
- [19] Zhang G, Fandrey C, Naqwi A, Wiedmann TS. High-frequency ultrasonic atomization for drug delivery to rodent animal models – optimal particle size for lung inhalation of difluoromethyl ornithine. *Exp Lung Res* 2008;34(5):209–23.
- [20] Liao X, Liang W, Wiedmann T, Wattenberg L, Dahl A. Lung distribution of the chemopreventive agent difluoromethylornithine (DFMO) following oral and inhalation delivery. *Exp Lung Res* 2004;30(8):755–69.
- [21] Xie Y, Longest PW, Xu YH, Wang JP, Wiedmann TS. In vitro and in vivo lung deposition of coated magnetic aerosol particles. *J Pharm Sci* 2010;99(11):4658–68.
- [22] Corti C, Pratesi G, DeCesare M, Pellegrini R, Giardini R, Supino R, et al. Spontaneous lung metastases in a human lung tumor xenograft: a new experimental model. *J Cancer Res Clin Oncol* 1996;122(3):154–60.
- [23] Hastings RH, Summers-Torres D. Direct laryngoscopy in mice. *Contemp Top Lab Anim Sci* 1999;38(6):33–5.
- [24] Frank JA, Kalish H, Jordan EK, Anderson SA, Pawelczyk E, Arbab AS. Color transformation and fluorescence of Prussian blue-positive cells: implications for histologic verification of cells labeled with superparamagnetic iron oxide nanoparticles. *Mol Imaging* 2007;6(3):212–8.
- [25] Taratula O, Garbuzenko OB, Chen AM, Minko T. Innovative strategy for treatment of lung cancer: targeted nanotechnology-based inhalation co-delivery of anticancer drugs and siRNA. *J Drug Target* 2011;19(10):900–14.
- [26] Drazen JM, Finn PW, De Sanctis GT. Mouse models of airway responsiveness: physiological basis of observed outcomes and analysis of selected examples using these outcome indicators. *Annu Rev Physiol* 1999;61:593–625.
- [27] Chen C, Hayek S, Mohite V, Yuan H, Chatterjee J, Haik Y. Nanomagnetism and magnetic hyperthermia. In: Nalwa HS, Webster T, editors. *Cancer nanotechnology: nanomaterials for cancer diagnosis and therapy*. San Diego, CA: American Scientific; 2007. p. 160–91.
- [28] Hu R, Ma S, Li H, Ke X, Wang G, Wei D, et al. Effect of magnetic fluid hyperthermia on lung cancer nodules in a murine model. *Oncol Lett* 2011;2(6):1161–4.
- [29] Hu R, Zhang X, Liu X, Xu B, Yang H, Xia Q, et al. Higher temperature improves the efficacy of magnetic fluid hyperthermia for Lewis lung cancer in a mouse model. *Thorac Cancer* 2012;3(1):34–9.
- [30] Jaracz S, Chen J, Kuznetsova LV, Ojima I. Recent advances in tumor-targeting anticancer drug conjugates. *Bioorg Med Chem* 2005;13(17):5043–54.
- [31] Garbuzenko OB, Saad M, Betigeri S, Zhang M, Vetcher AA, Soldatenkov VA, et al. Intratracheal versus intravenous liposomal delivery of siRNA, antisense oligonucleotides and anticancer drug. *Pharm Res* 2009;26(2):382–94.
- [32] Yi D, Naqwi A, Panoskaltis-Mortari A, Wiedmann TS. Distribution of aerosols in mouse lobes by fluorescent imaging. *Int J Pharm* 2012;426(1–2):108–15.
- [33] Raabe OG, Al-Bayati MA, Teague SV, Rasolt A. Regional deposition of inhaled monodisperse coarse and fine aerosol particles in small laboratory animals. *Ann Occup Hyg* 1988;32:53–63.
- [34] Beck SE, Laube BL, Barberena CI, Fischer AC, Adams RJ, Chesnut K, et al. Deposition and expression of aerosolized rAAV vectors in the lungs of *Rhesus macaques*. *Mol Ther* 2002;6(4):546–54.
- [35] Brown E, McKee T, diTomaso E, Pluen A, Seed B, Boucher Y, et al. Dynamic imaging of collagen and its modulation in tumors in vivo using second-harmonic generation. *Nat Med* 2003;9(6):796–800.
- [36] Eikenes L, Bruland ØS, Brekken C, Davies CDL. Collagenase increases the transcapillary pressure gradient and improves the uptake and distribution of monoclonal antibodies in human osteosarcoma xenografts. *Cancer Res* 2004;64(14):4768–73.